LETTERS

Tremor-tide correlations and near-lithostatic pore pressure on the deep San Andreas fault

Amanda M. Thomas[1], Robert M. Nadeau[1] & Roland Bürgmann[1]

Since its initial discovery nearly a decade ago[1], non-volcanic tremor has provided information about a region of the Earth that was previously thought incapable of generating seismic radiation. A thorough explanation of the geologic process responsible for tremor generation has, however, yet to be determined. Owing to their location at the plate interface, temporal correlation with geodetically measured slow-slip events and dominant shear wave energy, tremor observations in southwest Japan have been interpreted as a superposition of many low-frequency earthquakes that represent slip on a fault surface[2,3]. Fluids may also be fundamental to the failure process in subduction zone environments, as teleseismic and tidal modulation of tremor in Cascadia and Japan and high Poisson ratios in both source regions are indicative of pressurized pore fluids[3–7]. Here we identify a robust correlation between extremely small, tidally induced shear stress parallel to the San Andreas fault and non-volcanic tremor activity near Parkfield, California. We suggest that this tremor represents shear failure on a critically stressed fault in the presence of near-lithostatic pore pressure. There are a number of similarities between tremor in subduction zone environments, such as Cascadia and Japan, and tremor on the deep San Andreas transform[3–12], suggesting that the results presented here may also be applicable in other tectonic settings.

Analysis of the response of non-volcanic tremor to small stress oscillations induced in the lithosphere by the Earth's tidal deformation allows the determination of the stress orientations and magnitudes under which tremors preferentially occur, providing additional insight into the frictional processes that control tremor generation. Tidal modulation of tremor was previously established in both Japan and Cascadia[4,6,13,14]. The stresses induced by the ocean tides at these locations are nearly an order of magnitude larger than those near Parkfield[6,14], which primarily arise from the deformation of the solid Earth. We develop our analysis in parallel using a catalogue of 1,777 non-volcanic tremors detected over an eight-year period[11], a regional catalogue of earthquakes within 0.5° of Cholame, the central location of tremor activity, and a catalogue of characteristically repeating micro-earthquakes located along the creeping segment of the San Andreas fault, northwest of Cholame[15] (Fig. 1). We include the repeating earthquake catalogue because it is composed of events that are all located on the creeping San Andreas fault and might thus be expected to experience enhanced tidal triggering compared to regional catalogues[16]. We compute the extensional, shear and volume strains induced by the solid Earth and ocean tides[17,18], assuming a typical tremor source region depth of ~25 km (refs 11, 19). For each catalogue the fault-normal, shear, Coulomb (friction coefficient $\mu = 0.4$), and volumetric stresses and stress rates are computed for the times of each event (see Methods).

To investigate the influence of both the stress magnitude and rate on tremor and earthquake occurrence we divide the catalogue events into 'quadrants' depending on the sign of the loading condition under which they occur (Fig. 2, inset). If tremor and tides are uncorrelated, the number of events that occur under a particular tidal loading condition will be proportional to the amount of time that particular condition exists. Assuming each tremor event is independent, we use the chi-square statistic to test the null hypothesis that event times are randomly distributed with respect to tidal influence. The results for the tremor and earthquake catalogues are shown in Fig. 2. For the tremor catalogue, the levels of correlation of the normal, shear and Coulomb stresses exceed the 99% significance level while the correlation levels for the other catalogues are statistically insignificant. The lack of correlation in the regional and repeating earthquake catalogues is not surprising given the size of the catalogues and results from previous efforts to establish a significant tidal triggering of earthquakes[20–22] (see Methods).

We further explore the apparent correlation between tremor and tidally induced stresses by comparing tremor times with the loading conditions under which they occur. Figure 3 shows tremor rate distributions with respect to tidally induced shear, normal and Coulomb stress magnitudes and rates at the time of the events. Correlation between tremor occurrence and tidal stressing rate is insignificant for

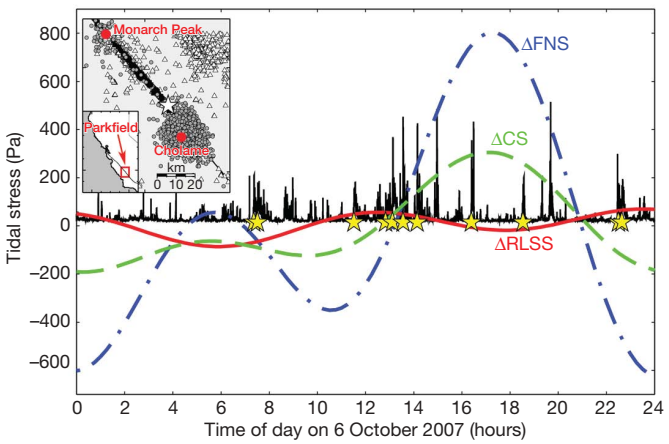

Figure 1 | Example one-day tremor time series with superimposed tidal stresses. Black represents root-mean-square envelope of tremor activity in Cholame. Blue, red and green curves represent the tidally induced fault-normal stress (ΔFNS), right-lateral shear stress (ΔRLSS), and Coulomb stress (ΔCS) for $\mu = 0.4$. Yellow stars mark tremor start times. Some short spikes in the root-mean-square envelope are due to micro-earthquakes. The inset map shows tremor locations as grey circles, locations of regional earthquakes as white triangles, and part of the repeating earthquake catalogue as black squares. Not all repeating events are shown, because they continue further to the northwest along the creeping San Andreas section. The white star indicates the epicentre of the 2004 Parkfield earthquake.

[1]Department of Earth and Planetary Science, Berkeley Seismological Laboratory, University of California-Berkeley, 307 McCone Hall, Berkeley, California 94720–4767, USA.

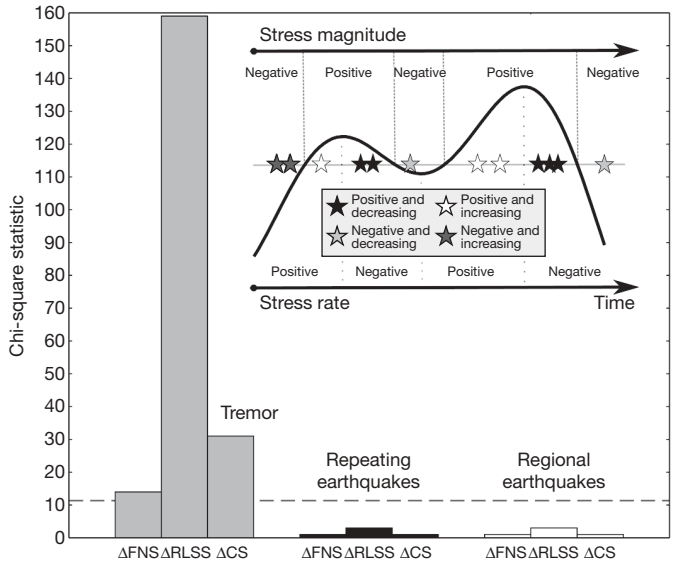

Figure 2 | Results of chi-square significance tests. The chi-square test results correlate the tremor, regional and repeating earthquake catalogues with tidally induced ΔFNS, ΔRLSS, and ΔCS. The dashed line shows the 99% confidence level, where larger values indicate that the hypothesis of random event occurrence can be rejected. The inset shows how tremor start times were separated into four 'quadrants' based on both the magnitude and rate of change of the stresses.

all stress components. Induced right-lateral shear stresses (ΔRLSS) demonstrates the most compelling correlation, with distinct increases in tremor activity that correspond to positive (right-lateral) shear stresses parallel to the San Andreas fault and equally apparent decreases when values are negative. Additionally, the tremor surpluses and deficits become more pronounced as ΔRLSS increases to values of ±150 Pa. Although fault-normal stress changes (ΔFNS) are much larger, they only exhibit a weak correlation at large, positive (tensile) values of >1,000 Pa. Coulomb stresses ($\Delta CS = \mu\Delta FNS + \Delta RLSS$, $\mu = 0.4$) exhibit less correlation than the shear stress alone.

Assuming a frictional Coulomb failure process is an appropriate model for non-volcanic tremor, the optimal friction coefficient μ is the value that maximizes the number of events that occur during times of encouraged failure stress (Fig. 4, Methods). Tremors show a marked increase for friction values of $\mu < 0.1$ with a peak of over 31% above the long-term average number of events (excess) for $\mu = 0.02$. The percentage excess for both the regional and repeating earthquake catalogues does not exceed 6%. This demonstrates that tidally induced shear stress parallel to the San Andreas fault, although of much smaller magnitude than normal stress changes, has the most robust correlation with non-volcanic tremor near Parkfield. The dominant role of small shear stress perturbations in stimulating the tremor, despite much larger normal stress perturbations, is indicative of a very weak fault zone with low effective normal stress, probably due to near-lithostatic pore pressures at the depth of the tremor source region. As a test of our assumption of San Andreas fault alignment in the stress calculations, we perform the same analysis to determine the percentage excess tremor with respect to a range of vertical fault plane azimuths (Fig. 4, inset). The peak percentage excess occurs at N 44° W, nearly parallel to the local strike of the San Andreas fault (N 45° W). This result serves as an independent piece of evidence to show that tremor represents a mode of fault-parallel shear failure in the lower crust.

If non-volcanic tremor simply represents a different class of earthquakes that still involves failure on a fault surface[13,23], it is unclear why tremor is modulated by tides but regional earthquakes are not. Careful statistical analyses of tidal influence on earthquake populations find the correlation to be extremely weak (~13,000 events are needed to establish a 1% increase)[20–22,24]. Lockner and Beeler[20,21] conducted a series of laboratory tests simulating tidal loading conditions on active faults and found that the absence of strong tidal triggering can be reconciled with rate-state frictional models that involve delayed slip nucleation (for example, by time-dependent failure or static fatigue). If tremor can also be described in a rate-state friction framework then we can derive a quantitative estimate of effective normal stress in the tremor source region from the observed tidal correlations[16]. Dieterich[16] found a simple scaling relationship between earthquake rate fluctuations and the amplitude of the

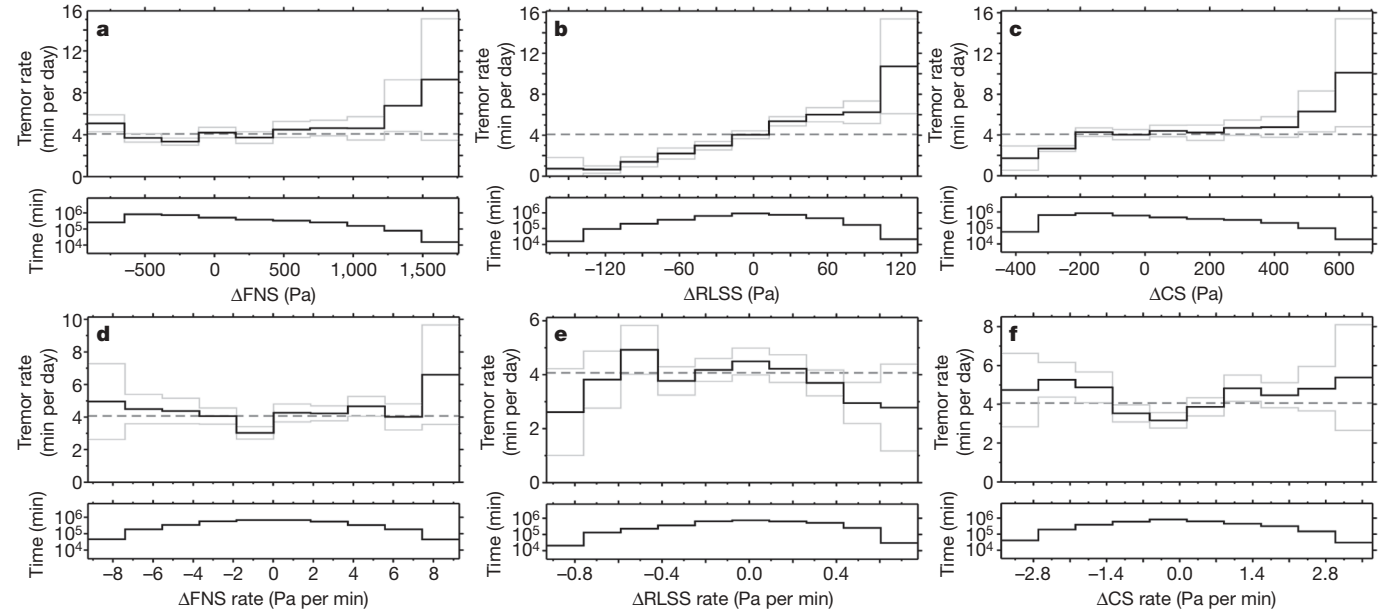

Figure 3 | Tidal stress magnitude and rate distributions. Tidal stress magnitude (panels **a**, **b** and **c**) and rate (panels **d**, **e** and **f**) distributions for the ΔFNS, ΔRLSS and ΔCS ($\mu = 0.4$). Volumetric stresses are not shown because they are strongly coupled with normal stresses. Solid black lines show tremor rates computed by dividing the number of tremors within the respective stress interval by the total amount of time spent in that interval. The time distribution for each bin is shown below each histogram. The average tremor rate (dashed line) corresponds to the rate expected if there were no correlation between tremor and tides. Grey lines are 2σ error bars (Methods).

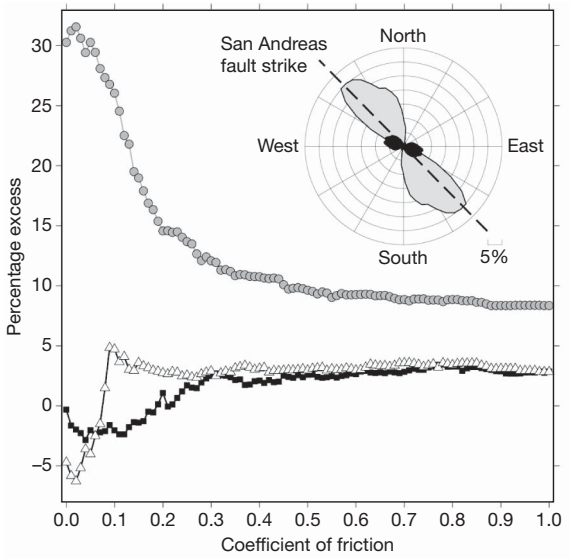

Figure 4 | Percentage of excess events versus friction coefficient. Percentage of excess events (that is, above long-term average) during times of positive ΔCS versus effective coefficient of friction. Values for the tremor, regional and repeating earthquake catalogues are shown as grey circles, white triangles and black squares respectively. Standard deviations (2σ) were computed using a bootstrap procedure on each friction value for each catalogue. Maximum 2σ errors over all possible friction values are 5.66%, 5.80% and 4.66% for the tremor, regional and repeating earthquake catalogues respectively. The inset displays the positive percentage excess tremor for ΔFNS (black) and ΔRLSS (grey) as a function of the fault azimuth.

periodic shear stress divided by the normal stress:

$$\sigma = 2\tau/(aR_a) \quad (1)$$

where R_a is the total rate variation divided by the average rate, $R_a = (R_{max} - R_{min})/R_{avg}$, σ is the effective normal stress, τ is the shear stress, and a is the rate constitutive parameter. Using the maximum and minimum rates for $\mu = 0.02$, the value of friction that maximizes the percentage excess (Supplementary Fig. 1), a stressing amplitude of 177 Pa (the maximum value of the tidally induced shear stress) and experimentally derived values of 0.005 to 0.02 for the fault constitutive parameter a (ref. 25), we find effective normal stresses of 0.035 to 0.009 MPa (Methods). These values are orders of magnitude lower than the lithostatic overburden pressure at this depth (~700 MPa), suggesting that effectively lithostatic pore fluids are present in the tremor source region. Additionally, this estimate is consistent with the low friction coefficient reflected in the lack of correlation with larger normal stress fluctuations. Potential sources of fluids at mid-crustal depths beneath the San Andreas fault are less well documented than slab dehydration in subduction zones, but previous studies have suggested the presence of fluids and processes to explain their introduction[26].

The similarities (or differences) in non-volcanic tremor properties with respect to tectonic environment warrant further discussion. Nakata *et al.*[6] suggest correlation with ΔCS (assuming $\mu = 0.2$) and ΔCS rate in Shikoku, Japan, while Lambert *et al.*[14] find that peak tremor activity occurs at times of maximum tidal shear stress in the thrust direction and with ΔCS (assuming $\mu = 0.4$) in Cascadia. One possible reason for the different results is that both in Japan (R. Nakata, personal communication, 2009) and Cascadia[14] times of increased shear stress are highly correlated with compressive (clamping) normal stresses of comparable magnitude. This makes it difficult to separate the individual contributions of the normal and shear stresses, especially for the short time periods (a few weeks) considered by these two studies. The results for Parkfield are not subject to this limitation and we find that very small shear stresses, but not the larger normal stress changes, modulate tremor. It is likely that tremor modulation is affected by frictional strength, the relative magnitude of tectonic and tidal loading rates[20,21], material properties[5], and other factors that vary with respect to tectonic environment. One finding common to all three localities is that tremor appears to be associated with the presence of fluids at near-lithostatic pressures, and given similar observations in variable tectonic environments[3–6], the same mechanism is probably responsible for non-volcanic tremor elsewhere.

We find that tremor occurs preferentially when subjected to tidal shear stresses that promote right-lateral failure along the San Andreas fault, very small stress perturbations from solid-Earth tides are responsible for significant tremor rate increases, and extremely low effective normal stress in the tremor source region is required to explain the apparent tidal triggering. Tremor appears to be shear failure capable of producing seismic radiation, so a brittle failure model seems appropriate. These results present a rheological paradox, because ductile rheologies, which may be expected at depths of more than 20 km and temperatures over 500 °C, generally have no normal-stress dependence. It is possible that very high fluid pressures on discrete fault patches facilitate slip in an otherwise ductile-deforming regime. Coupling these observations with the location of the tremor on deep, roughly planar zones[19], we favour the conjecture that tremor at Cholame represents shear failure within a weak, critically stressed San Andreas fault zone extending to the base of the crust. Finally, given that earthquakes and non-volcanic tremor are both manifestations of slip on a fault surface, further constraining the properties and processes that control tremor generation may facilitate a better understanding of fault mechanics, lithospheric structure and tectonic deformation in the deep crust.

METHODS SUMMARY

Tidal stress computation. Tidally induced strains are computed in the tremor source region using SPOTL[17,18]. Assuming two-dimensional plane strain and linear elasticity, with an elastic modulus of 30 GPa and Poisson ratio of 0.25, strains are then converted to stresses and resolved into fault normal and parallel (shear) directions of the San Andreas fault (N 45° W).

Effective normal stress computation. The stress histogram for friction coefficient $\mu = 0.02$ (the value of the friction coefficient that maximizes the percentage excess from Fig. 4) is shown in Supplementary Fig. 1. From this figure the maximum and minimum tremor rates are 9 min per day and 1 min per day, respectively. Using expression (1) in the text we find that $R_a = 2$, resulting in effective normal stress estimates of 35,400 Pa and 8,850 Pa for a values of 0.005 and 0.02 respectively.

Full Methods and any associated references are available in the online version of the paper at www.nature.com/nature.

Received 30 April; accepted 3 November 2009.

1. Obara, K. Nonvolcanic deep tremor associated with subduction in southwest Japan. *Science* **296,** 1679–1681 (2002).
2. Shelly, D. R., Beroza, G. C. & Ide, S. Non-volcanic tremor and low-frequency earthquake swarms. *Nature* **446,** 305–307 (2007).
3. Shelly, D. R., Beroza, G. C., Ide, S. & Nakamula, S. Low-frequency earthquakes in Shikoku, Japan, and their relationship to episodic tremor and slip. *Nature* **442,** 188–191 (2006).
4. Rubinstein, J. L., La Rocca, M., Vidale, J. E., Creager, K. C. & Wech, A. G. Tidal modulation of nonvolcanic tremor. *Science* **319,** 186–189 (2008).
5. Audet, P., Bostock, M. G., Christensen, N. I. & Peacock, S. M. Seismic evidence for overpressured subducted oceanic crust and megathrust fault sealing. *Nature* **457,** 76–78 (2009).
6. Nakata, R., Suda, N. & Tsuruoka, H. Non-volcanic tremor resulting from the combined effect of Earth tides and slow slip events. *Nature Geosci.* **1,** 676–678 (2008).
7. Gomberg, J. *et al.* Widespread triggering of nonvolcanic tremor in California. *Science* **319,** 173 (2008).
8. Rogers, G. & Dragert, H. Episodic tremor and slip on the Cascadia subduction zone: the chatter of silent slip. *Science* **300,** 1942–1943 (2003).
9. Brenguier, F. *et al.* Postseismic relaxation along the San Andreas fault at Parkfield from continuous seismological observations. *Science* **321,** 1478–1481 (2008).
10. Rubinstein, J. L. *et al.* Non-volcanic tremor driven by large transient shear stresses. *Nature* **448,** 579–582 (2007).
11. Nadeau, R. M. & Guilhem, A. Nonvolcanic tremor evolution and the San Simeon and Parkfield, California, earthquakes. *Science* **325,** 191–193 (2009).
12. Nadeau, R. M. & Dolenc, D. Nonvolcanic tremors deep beneath the San Andreas fault. *Science* **307,** 389 (2005).

13. Shelly, D. R., Beroza, G. C. & Ide, S. Complex evolution of transient slip derived from precise tremor locations in western Shikoku, Japan. *Geochem. Geophys. Geosyst.* **8,** doi:10.1029/2007gc001640 (2007).
14. Lambert, A., Kao, H., Rogers, G. & Courtier, N. Correlation of tremor activity with tidal stress in the northern Cascadia subduction zone. *J. Geophys. Res. Solid Earth* **114,** doi:10.1029/2008JB006038 (2009).
15. Nadeau, R. M. & McEvilly, T. V. Periodic pulsing of characteristic microearthquakes on the San Andreas fault. *Science* **303,** 220–222 (2004).
16. Dieterich, J. H. Nucleation and triggering of earthquake slip—effect of periodic stresses. *Tectonophysics* **144,** 127–139 (1987).
17. Agnew, D. *SPOTL: Some Programs for Ocean Tide Loading* ⟨http://igppweb.ucsd.edu/~agnew/spotlmain.html⟩ (1996).
18. Agnew, D. C. NLOADF: A program for computing ocean-tide loading. *J. Geophys. Res. Solid Earth* **102,** 5109–5110 (1997).
19. Shelly, D. R. *et al.* Precise location of San Andreas fault tremors near Cholame, California using seismometer clusters: slip on the deep extension of the fault? *Geophys. Res. Lett.* **36,** doi:10.1029/2008gl036367 (2009).
20. Beeler, N. M. & Lockner, D. A. Why earthquakes correlate weakly with the solid Earth tides: effects of periodic stress on the rate and probability of earthquake occurrence. *J. Geophys. Res. Solid Earth* **108,** doi:10.1029/2001jb001518 (2003).
21. Lockner, D. A. & Beeler, N. M. Premonitory slip and tidal triggering of earthquakes. *J. Geophys. Res. Solid Earth* **104,** 20133–20151 (1999).
22. Vidale, J. E., Agnew, D. C., Johnston, M. J. S. & Oppenheimer, D. H. Absence of earthquake correlation with Earth tides: an indication of high preseismic fault stress rate. *J. Geophys. Res. Solid Earth* **103,** 24567–24572 (1998).
23. Ide, S., Shelly, D. R. & Beroza, G. C. Mechanism of deep low frequency earthquakes: further evidence that deep non-volcanic tremor is generated by shear slip on the plate interface. *Geophys. Res. Lett.* L03308 doi:10.1029/2006gl028890 (2007).
24. Cochran, E. S., Vidale, J. E. & Tanaka, S. Earth tides can trigger shallow thrust fault earthquakes. *Science* **306,** 1164–1166 (2004).
25. Blanpied, M. L., Lockner, D. A. & Byerlee, J. D. Frictional slip of granite at hydrothermal conditions. *J. Geophys. Res. Solid Earth* **100,** 13045–13064 (1995).
26. Becken, M. *et al.* A deep crustal fluid channel into the San Andreas Fault System near Parkfield, California. *Geophys. J. Int.* **173,** 718–732 (2008).

Supplementary Information is linked to the online version of the paper at www.nature.com/nature.

Acknowledgements We thank D. Agnew, N. Beeler, G. Beroza, F. Bonetto, J. Gomberg, A. Guilhem, R. Nakata, Z. Peng, E. Roeloffs and D. Shelly for discussion and comments that improved the manuscript. Funding was provided in part by the National Science Foundation through a Graduate Research Fellowship and awards EAR-0537641 and EAR-0544730, and by the US Geological Survey through awards 06HQGR0167, 07HQAG0014 and 08HQGR0100. Data used in this study were obtained from the Northern California Earthquake Data Center (NCEDC). This is Berkeley Seismological Laboratory contribution #10-23.

Author Contributions A.M.T. performed the analysis. A.M.T. and R.B. wrote the paper. R.M.N. developed the tremor and repeating earthquake catalogues and performed analysis related to Figure 3. All authors contributed to the interpretation and final manuscript preparation.

Author Information The authors declare no competing financial interests. Reprints and permissions information is available at www.nature.com/reprints. Correspondence and requests for materials should be addressed to A.M.T. (amthomas@berkeley.edu).

METHODS

Event catalogues. The tremor catalogue includes a total of 1,777 events between July 2001 and May 2008 using the detection methodology described in ref. 11. A small portion (5–10%) of the non-volcanic tremor occur farther north beneath Monarch Peak, but the tidally induced stresses do not vary in a significant way over such small distances, so tidal-stress time series were computed for Cholame only. The repeating earthquake catalogue contains 2,594 events between 1984 and 1999 on the 175-km creeping section of the San Andreas fault[15]. The tidal stresses for this catalogue were computed at the centre of the creeping section at 5 km depth. Finally, the regional earthquake catalogue consists of all earthquakes from the Advanced National Seismic System catalogue, for the same time period as the tremor catalogue, that are within 0.5° from the centre of the Cholame tremor. The same tidal time series were used for the tremor and regional earthquakes and were computed at 35.666° N, 120.2854° W.

Tidal stress calculation. The tidally induced stresses in the lithosphere were computed using the SPOTL code developed by D. Agnew[17,18]. SPOTL uses Green's functions to compute azimuthal and vertical strains that can subsequently be converted to stress. A more thorough description of the mathematical treatment of tides and code specifics can be found on the SPOTL webpage (http://www.igpp.ucsd.edu/~agnew/spotlmain.html). The results in this analysis include contributions from both the body tides, which arise due to deformation of the solid Earth, and the ocean load tides. The computation includes the semi-diurnal M2, N2, S2 and K2, and diurnal K1, O1, P1 and Q1 tidal constituents and we used the TOPEX/Poseidon global ocean tide model included in the SPOTL package to compute the load tides. Tidal model predictions were compared with strain-meter records in Piñon Flat using the perturbation matrix of ref. 27, as well as previous studies to verify the calculation[22,27].

Statistical methods. Pearson's chi-square test is designed to test the similarity between two frequency distributions[28]. The measure of similarity is known as the chi-squared statistic and is defined as:

$$\chi^2 = \sum_{i=1}^{n} \frac{(O_i - E_i)^2}{E_i} \quad (2)$$

where n is the total number of potential outcomes, O_i is the observed frequency for a particular outcome i, and E_i is the expected frequency for a particular outcome[28]. In the case of non-volcanic tremor, the total number of tremors are each assigned to one of four possible categories or 'quadrants' (positive and decreasing, negative and decreasing, and so on) depending on the behaviour of the tidally induced stress under consideration at the time the tremor occurred. The expected number is computed by taking the entire eight-year tidal time series and determining what fraction of time was spent in each group, then multiplying by the total number of tremors in the catalogue. In this way we account for the fact that the time distribution is not equivalent between quadrants. The grey dashed line in Fig. 2 is the critical value (99% significance level) for an upper one-sided test with three degrees of freedom.

Each tremor in Fig. 3 is weighted by its duration so, for example, one 15-min tremor is equivalent to three 5-min tremors. This is in contrast to Figs 2 and 4, where all tremors are weighted equally. We chose this approach because the tremor rates can then be used to compute an effective normal stress in the tremor source region.

Figure 4 again weights all tremors equally and is somewhat analogous to the chi-square tests mentioned earlier. The percentage excess is defined as $(O - E)/E$, using the same observed and expected values (O and E) as in the chi-square test, but in the case of Fig. 4 we consider only the positive magnitudes ($n = 1$). The percentage excess is roughly related to the chi-square values, the main difference being that the chi-square is a measure of the variance of a population whereas the percentage excess is related to the mean. Two populations of different size with the same percentage excess (10 coin flips with 6 heads and 1,000 coin flips with 600 heads, for example) will have greatly different chi-square statistics. The larger population will have the highest chi-square value because it is much more statistically improbable.

Uncertainty estimates from Fig. 3. Two-standard-deviation error estimates are determined using a bootstrap method. The method randomly selects an individual tremor from the original tremor catalogue of 1,777 tremors. This process is repeated 1,777 times to yield a randomly sampled catalogue (with replacement) of 1,777 events. The above process is repeated 50 times, giving 50 randomly sampled versions of the original catalogue. The tremor rate distributions as a function of the tidally induced stresses are then calculated for each of the 50 randomly sampled catalogues. For each stress bin, the standard deviation of tremor rates of the 50 catalogue values are then computed and multiplied by 2, giving the 2σ rate uncertainties for each bin that are shown by the grey bars in Fig. 3. Tremor rate errors arise from variability in tremor detection sensitivity. More details on the detection methodology can be found in ref. 11.

27. Hart, R. H. G. *et al.* Tidal calibration of borehole strainmeters: removing the effects of small-scale inhomogeneity. *J. Geophys. Res.* **101,** 25553–25571 (1996).
28. Devore, J. L. *Probability and Statistics: for Engineering and the Sciences* 6th edn, Ch. 14 (Brooks/Cole-Thomson Learning, 2004).